When cells respond to light

All you need is LOV

Van Geel, O.

Publication date
2020
Document Version
Other version
License
Other

[Link to publication](#)

Citation for published version (APA):

Van Geel, O. (2020). *When cells respond to light: All you need is LOV*. [Thesis, fully internal, Universiteit van Amsterdam].

CHAPTER 3

Combining optogenetics with sensitive FRET imaging:
A readout for local microtubule manipulation

Orry Van Geel[1], Stephanie Cheung[1,2] & Theodorus W.J. Gadella[1]

[1]Swammerdam Institute for Life Sciences, Section of Molecular Cytology, van Leeuwenhoek Centre for Advanced Microscopy, University of Amsterdam, Science Park 904, 1098XH Amsterdam, The Netherlands.

[2]Developmental Biology Unit, European Molecular Biology Laboratory, 69117 Heidelberg, Germany.

Abstract

Optogenetic methods for switching molecular states in cells is an increasingly prominent tool in life sciences. Förster Resonance Energy Transfer (FRET)-based sensors can provide quantitative and sensitive readouts of altered cellular biochemistry, e.g. from optogenetics. However, most of the light-inducible domains respond to the same wavelength as is required for excitation of popular CFP/YFP-based FRET pairs, rendering the techniques incompatible with each other. In order to overcome this limitation, we red-shifted the existing CFP/YFP-based COPY FRET sensor by employing an sYFP2 donor and mScarlet-I acceptor. Their favorable quantum yield and brightness result in a red-shifted FRET pair with an optimized dynamic range, which could be further enhanced by an R125I point mutation that stimulates intramolecular interactions. The new sensor was named ROPY and it visualizes the interaction between the microtubule regulator stathmin/OP18 and free tubulin heterodimers. We show that through phosphorylation of the ROPY sensor, its tubulin sequestering ability can be locally regulated by photo-activatable Rac1 (PARac1), independent of the FRET readout. Together, ROPY and PARac1 provide spatiotemporal control over free tubulin levels. ROPY/PARac1-based optogenetic regulation of free tubulin levels allowed us to demonstrate that depletion of free tubulin prevents the formation of pioneer microtubules, while local upregulation of tubulin concentration allows localized microtubule extensions to support the lamellipodia.

Introduction

The field of optogenetics is continually expanding, producing a steady stream of new light responsive tools and applications with an increasing impact on science[1,2,3]. Most of the optogenetic tools contain protein domains that perform their function in response to light from the blue end of the spectrum, e.g. LOV domains, channelrhodopsins, cryptochromes, etc.[1,4] Unfortunately, the same part of the spectrum is used for another popular technique in microscopy as well, namely *Förster resonance energy transfer* (*FRET*). Most FRET sensors are developed with cyan and yellow fluorescent protein (FP) pairs since they have good characteristics for FRET imaging based on donor quenching and acceptor sensitization[5,6]. In order to combine blue-sensitive optogenetics with FRET imaging, more red-shifted fluorophores are needed to avoid crosstalk from overlapping excitation windows. The donor needs to be excited above 514 nm, which rules out the use of cyan FPs. Yellow FPs like mVenus, SYFP2, mCitrine or orange FPs like mKO or mOrange fulfill this requirement. For these donors, red FPs or far red FPs are required as acceptor, respectively. However, (far) red fluorescent proteins have historically been compromised with low quantum yields and/or maturation problems, hampering robust and efficient red-shifted FRET sensors. Recently, improved red FPs have been developed that allow for novel and efficient FRET sensing with red-shifted spectral properties[7]. We utilized these improved red FPs for creating a suitable red-shifted FRET pair

that can be efficiently excited at 514 nm[7,8]. To this end we incorporated new red-shifted FRET pairs into the COPY sensor, which originally had a YFP/CFP pair attached to the N- and C-terminus of a stathmin/oncoprotein18 (OP18) molecule[9]. Stathmin is an important negative regulator of microtubule dynamics[10,11], and will shift the dynamic instability of microtubules towards depolymerization when it captures free tubulin dimers in a 2:1 ratio[12]. This tubulin sequestering function is believed to be the driving force behind the stimulation of microtubule catastrophes[10]. Although the N-terminal part is known to interact with microtubule tips as well, which can potentially stimulate depolymerization to some extent[13,14]. There are four serine residues that can become phosphorylated in stathmin via a number of cellular signaling pathways, among which is the Rac1-PAK1 pathway[15,16,17]. Phosphorylation diminishes stathmin's affinity for tubulin and its tertiary structure shifts from a large elongated α-helix to an unstructured chain[18]. Stathmin's control over tubulin availability is critical in a number of cellular processes like mitosis[9,19], and helps to tightly regulate the balance of microtubule dynamics in cooperation with the other microtubule regulatory factors[20]. So far, the effect of stathmin has only been studied through stimulation of entire cells[9,13,21], whereas it is known that microtubule dynamics are typically regulated locally. In this study we aimed to generate a new optogenetic application with FRET readout to allow simultaneous local control of microtubule dynamics and monitoring of local free tubulin concentrations. To this end we created a novel red-shifted stathmin sensor we termed ROPY. We show the compatibility of the ROPY FRET sensor with blue light responsive optogenetics and demonstrate that localized release of tubulin can stimulate microtubule growth in that area.

Results

Generating a red-shifted FRET sensor with suitable dynamic range

The original CFP/YFP-based COPY sensor is not suitable for experiments with blue light responsive optogenetics due to the impossibility to excite the donor without activating the optogenetic module. We aimed to simultaneously manipulate and monitor the free tubulin concentration by using an asLOV2-based optogenetic switch[22] in combination with FRET. Hence, we needed to red-shift the fluorescent proteins used in the COPY sensor to ones that can be excited above 500nm (fig 1A). The COPY sensor reports on the difference between the monomeric disordered stathmin state where the terminal FPs can interact, and the stabilized elongated α-helix through the binding of tubulin where the terminal FPs are too far apart to interact[9,18]. Such changes in FRET can be induced by altering stathmin's tubulin-binding properties through phosphorylation or by modulating the intracellular free tubulin concentration, for instance with a drug like paclitaxel which prevents microtubule depolymerization[21] (fig 1B). In a first attempt we combined orange fluorescent protein donors
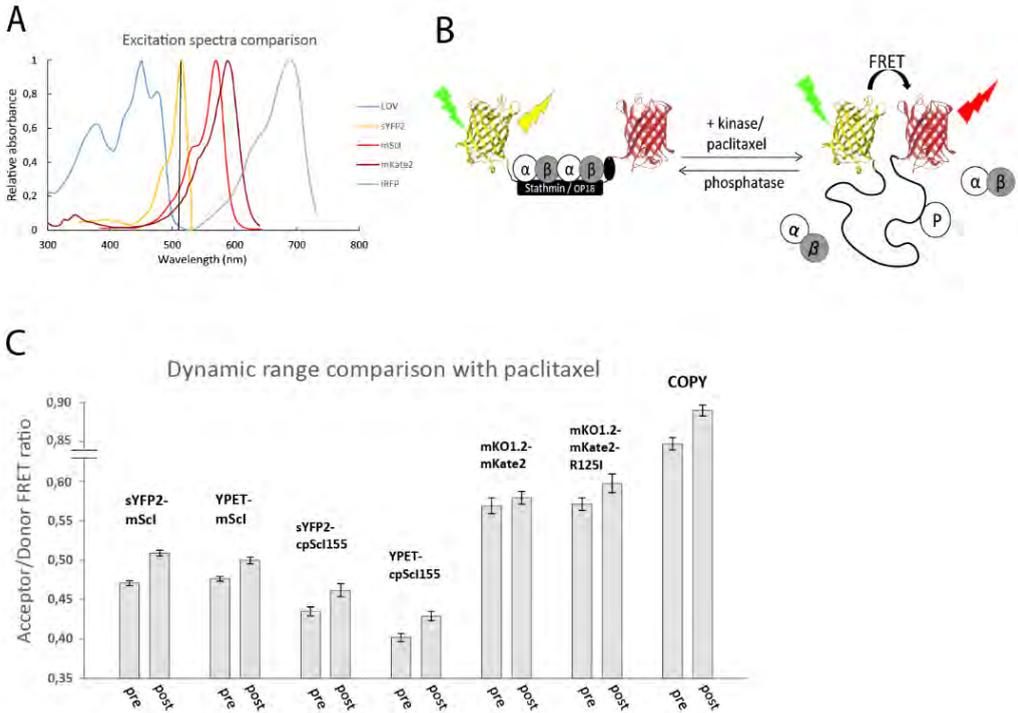
Fig 1. Generating a red-shifted FRET sensor with suitable dynamic range. (A) The excitation spectrum of a common blue-responsive optogenetics domain is plotted together with the fluorescent proteins used in this study to indicate the minimal amount of spectral overlap present. (B) Schematic overview of how the stathmin FRET-sensor cycles between elongated and unstructured states depending on tubulin binding. (C) Ratiometric FRET comparison of several FP combinations we tested, before and after addition of 10 μM paclitaxel. The sensors were transiently expressed in HEK293T cells and averages for each condition were calculated from n>400 cells. Error bars indicate the 95% confidence intervals.

Table 1	Relative FRET increase
sYFP2-mScI	1,081 ± 0,015
YPET-mScI	1,049 ± 0,016
YPET-cpSc155	1,068 ± 0,028
sYFP2-cpSc155	1,062 ± 0,032
mKO1.2-mKate2	1,017 ± 0,031
mKO1.2-mKate2-R125I	1,046 ± 0,035
COPY	1,065 ± 0,024
ROPY-4A	1,146 ± 0,021
ROPY	1,113 ± 0,022
ROPY-4E	1,014 ± 0,016
ROPY-Y67Gs	0,998 ± 0,025
ROPY (DMSO)	1,007 ± 0,018

Table 1 Overview of relative FRET ratio changes upon paclitaxel stimulation.

Values were obtained by subtracting the normalized average FRET ratios before and after paclitaxel addition, represented with ± 95% confidence interval of n>400 for each condition.

with near-infrared fluorescent protein acceptors, yet we could not find a combination with a dynamic range above background noise (fig 1C). This is partly due to the sensor's design displaying an intrinsically low dynamic range, and in part related to poor quantum yield and maturation problems of the employed acceptor FP probes. We therefore decided to focus on FP pairs which can elicit the maximum theoretical FRET potential in the desired excitation range, i.e. a donor FP with high quantum yield with optimal excitation at 514 nm and acceptor with high brightness and efficient maturation[6,8]. mScarlet-I (mScI) was chosen as the best FRET acceptor currently available in the red spectrum[7] and we combined it with yellow FPs either Ypet[23] or sYFP2[24]. The excitation spectra show that activation of YFP at 514nm can theoretically still slightly trigger the edge of the LOV spectrum as well (fig1A), however in our experience this did not activate the LOV domain in any detectable way if the laser intensity was kept low. We compared ratiometric FRET changes of both wildtype and circular permutated versions of the red-shifted sensor upon adding 10 µM of paclitaxel for 1h that reduces the free tubulin concentration and hence enhances FRET (fig 1C). Altering the FP orientation with circular permutation did not improve the FRET interaction and it became clear that a sYFP2-mScI pair had the largest FRET response out of all the explored combinations (Table1). This FRET pair allows one additional orthogonal detection channel in the near-infrared part of the spectrum that can be used for localizing proteins of interest tagged by a near-infrared fluorescent probe, e.g. iRFP713 (fig 1A).

Optimization and characterization of the ROPY FRET sensor

Once we established the optimal sYFP2-mScI FRET pair for the stathmin sensor, we looked into modifying its properties in order to improve the dynamic range. Since the FRET interaction of the sensor is dependent on the proximity of both FPs in the tubulin unbound state, we attempted to reverse the monomeric mutation in coral derived FPs by introducing a R125I point mutation[25]. The mutation successfully increased the dynamic range in the coral derived mKO1.2-mKate2 pair (Table1), yet this pair was sub-optimal, so we also tried if the R125I mutation would have the same effect in mScarlet-I. Indeed, R125I successfully increased the dynamic range for mScI as well (fig 2A), and we named this final optimized version ROPY (RFP-OP18-YFP). Next, we were interested in determining whether the R125I mutation induced the higher FRET response through mScarlet homo-dimerization or through sYFP2-mScI hetero-dimerization. To this end, we introduced a Y67G point mutation into either sYFP2 or mScI which abolishes the formation of the FP-chromophore in either FP. Upon expressing a mix of ROPY sensors with chromophore-less sYFP2 and mScI proteins (fig S1), we found no FRET response after addition of paclitaxel (fig2A), which suggests that the increased FP interaction due to the R125I mutation is not intermolecular but intramolecular in nature. The fact that the baseline FRET ratios are similar further dismisses intermolecular interactions.
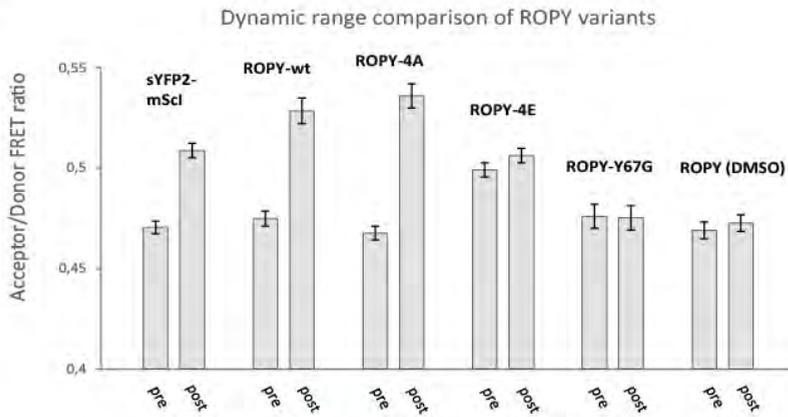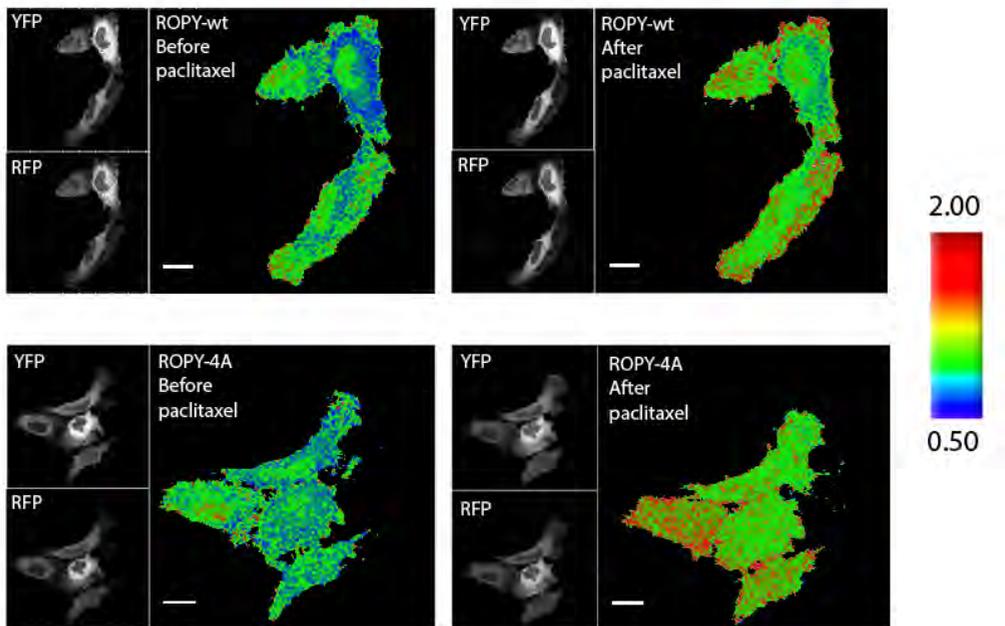
Fig 2. Optimization and characterization of new ROPY FRET sensor. (A) RFP/YFP ratiometric FRET comparison of several ROPY mutations, before and after addition of 10 µM paclitaxel, one control condition used DMSO without paclitaxel. The sensors were transiently expressed in HEK293T cells and averages for each condition were calculated from n>600 cells. Error bars indicate the 95% confidence intervals. (B) Confocal images of YFP and RFP emissions along with their RFP/YFP ratio for ROPY variants before and after 5 minutes of 10 µM paclitaxel addition. Experiment was performed in HeLa cells. Scale bars represent 20 µm.

We evaluated the properties of the ROPY sensor further by making a phospho-mimetic variant with four serines mutated into glutamic acids (ROPY-4E) and a phospho-blocking variant with four serines mutated into alanines (ROPY-4A), as previously reported in the literature[9,26]. Respectively, these mutants should minimize and maximize the sensor's affinity for tubulin, thereby indicating the lower and upper range of the ROPY sensor signal. Indeed, when we compared ratiometric FRET changes upon adding 10 µM of paclitaxel for 1h, we detected hardly any difference for ROPY-4E and a bigger difference for ROPY-4A as compared to the wildtype (fig 2A). This confirms that the regulatory tubulin sequestering ability of ROPY is still functioning like wildtype stathmin[9,16].

On a single cell scale, it becomes clear that the wildtype stathmin sensor has a more inhomogeneous spatial distribution of the FRET response than ROPY-4A (fig2B), which was detected with the original COPY sensor as well[9]. This suggests that endogenous phosphorylation of the sensor occurs mostly near the cell edges.

Interestingly, we observed a rising variability in the baseline FRET ratios with increasing ectopically expressed ROPY sensor concentrations (fig S2). Also the difference in FRET readout between ROPY-4E and ROPY-4A is greatly diminished at higher sensor concentrations (not shown), which could sometimes be a result of bystander FRET at elevated sensor concentrations. However, based on the negative result for intermolecular FRET we think it is more likely that in case of overexpression of the sensor, ROPY will titrate out the available free tubulin in the cell causing an increasingly lower tubulin occupancy of the sensor and thereby a reduction of FRET and sensitivity of the sensor.

Combining ROPY with blue responsive optogenetics

The next step was to test the compatibility of the new red-shifted ROPY sensor with a blue light responsive optogenetic construct, PARac1. The Rac1 Rho-GTPase affects many signaling pathways involved in cytoskeletal organization[27], including OP18 regulation (fig 3A). The spectral characteristics of ROPY allow for an additional fluorescent tag to be imaged in the far-red spectrum (fig 1A), so we co-expressed ROPY, PARac1 with an mTq2 fluorescent tag, and α-tubulin with an iRFP713 tag[28] (fig 3B). All channels except for CFP could be independently imaged while no response from PARac1 was detected during the baseline. The mTq2 tag could only be imaged during the activation step starting right after the final baseline image of the ROPY channels was taken, but this is enough to also detect the increase in PARac1 concentration at the plasma membrane during its activation. We illuminated the whole cell with 458nm light during 5 minutes, followed by 5 minutes recovery time in the dark. During this time we observed the FRET ratio increase in the entire cell followed by a decrease back to baseline levels. The subcellular inhomogeneous distribution of ROPY activity is present throughout all timepoints to varying degrees. Not only is the spatial FRET gradient usually highest near the edge of the cell, the largest increase in ratio over time also occurs at the edge (fig 3C). On average, the changes near the edge of the cell were almost twice as large as the

ones in the center. In order to confirm that the observed changes were due to the interplay between ROPY & PARac1, we measured negative controls where either the sensor could not be phosphorylated (ROPY-4A) or where Rac1 could not be activated (PARac1-C450A) and indeed we found no significant responses under those conditions (fig S3). This indicates that the changes seen in figure 3B reflect phosphorylation of the ROPY sensor through PARac1 optogenetic stimulation.
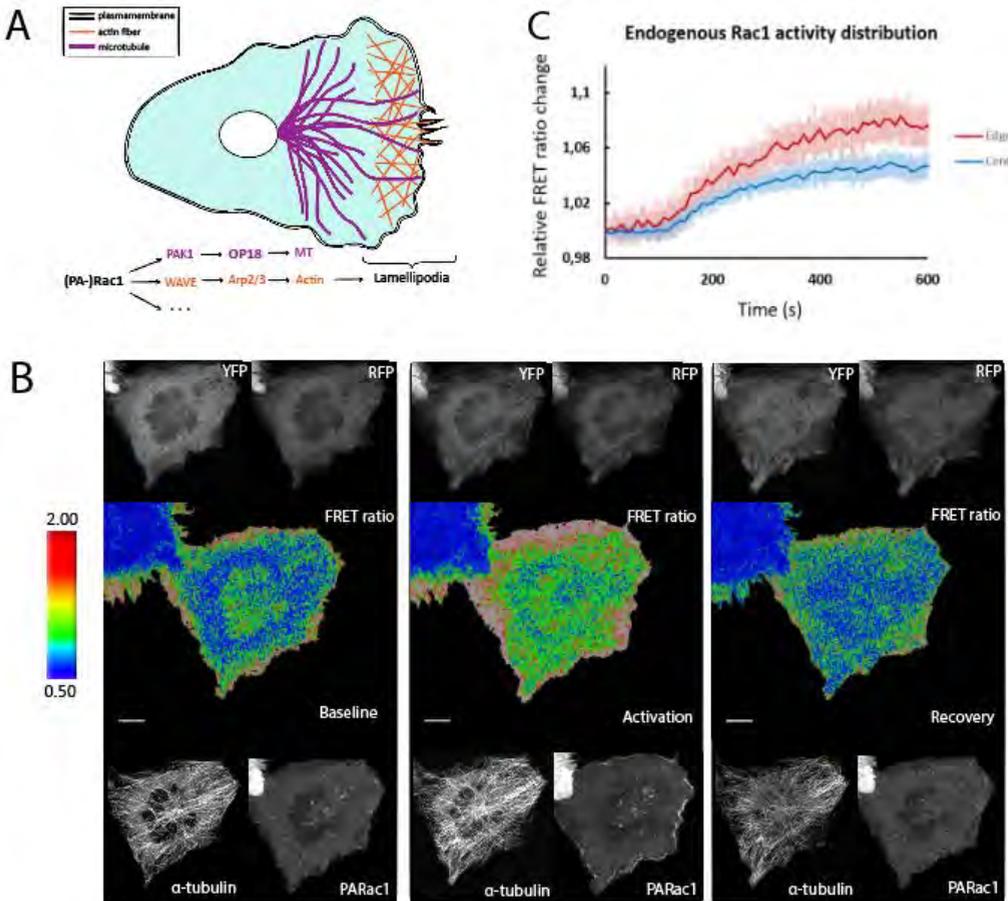

Fig 3. Combining ROPY with blue responsive optogenetics. (A) Schematic overview of the signaling pathways affected by Rac1 which result in cytoskeletal growth and lamellipodia formation. (B) Confocal images of ROPY, PARac1 & α-tubulin-iRFP co-expression in HeLa cells. Baseline was acquired in the dark state, the activation images were taken 5 minutes after illuminating the entire cell with 458nm pulses every 20s, and recovery images were taken 5 minutes after the last 458nm light pulse was given. Scale bars represent 10 μm (C) Normalized ratiometric ROPY changes over time in response to PARac1 activation. The FRET signal in HeLa cells was divided in an outer region of 5 μm thickness (red) and the remaining inner region (blue). Error bars represent the standard deviation, n=10.

Locally affecting the tubulin affinity of ROPY

The advantage of optogenetic constructs is that they can be locally activated, thus we examined the response of ROPY to a localized phosphorylation stimulus (fig 4A). PARac1 induced membrane ruffling and protrusions, which were most prominent in the area of 458nm illumination. This is explained through its modulatory effects on the actin cytoskeleton[27,29]. In contrast to the regional membrane ruffling following optogenetic Rac1 stimulation, we found that the ROPY sensor responds similarly to localized or non-localized stimuli, with a FRET increase throughout the entire cell and a gradient from the cell edge to the center (Fig 3A). This suggests that in the sequence of events leading to the phosphorylation-induced FRET response, certain components apparently display a diffusion rate that is high enough for the phosphorylated sensor to dominate the entire cellular response. This precludes that the combination of PARac1 and ROPY can be used to investigate how locally released tubulin affects the microtubule dynamics in combination with a clear readout of the area where tubulin was released through the sensor. We previously tackled the problem of maintaining spatial resolution with optogenetics[30], and sought to circumvent this problem in a similar way. We attempted to lower the diffusion of ROPY by adding two lactadherin-C2 lipid binding domains at the C-terminus (ROPY-2C2) that will keep it mostly bound to the plasma membrane[31]. Unlike free diffusing ROPY (fig 4A), the ROPY-2C2 version was able to indicate local activation gradients (Fig 4B). As a control we paired ROPY-4A with PARac1 and detected localized membrane protrusions, indicating Rac1 activation, without a change in stathmin activity as expected (Fig 4C). We show the disparity of local PARac1 activity detection between free ROPY and ROPY-2C2 for a handful of cells to indicate the need for this membrane bound version (fig 4D).

Now that we established a localized release of free tubulin under optogenetic control with FRET readout, we investigated how a localized increase in free tubulin would influence microtubule growth. As a way of visually confirming that tubulin is indeed being released upon stathmin phosphorylation, we locally activated PARac1 in cells expressing ROPY-2C2 and α-tubulin-iRFP. Indeed, we observed that colocalization of these proteins diminished within the area of illumination (fig S4). We studied the effect that locally releasing tubulin has on microtubules by expressing iRFP-tagged EB3 which has a high affinity for growing microtubule +TIPs[32]. We were able to detect microtubules beyond the original cell outline and into the PARac1 induced protrusions, shaping the form of the resulting lamellipodia (Fig 4 A,B), though not for cells expressing ROPY-4A (fig 4C). This implies that the microtubule extensions are a direct result of the local release of free tubulin dimers. These microtubule extensions correlate nicely with the areas of increased FRET activity. Protrusions outside of the illuminated region where ROPY-2C2 detected no FRET response did not exhibit this local microtubule growth effect (fig S5), indicating that most of the released tubulin is quickly incorporated into local microtubules.
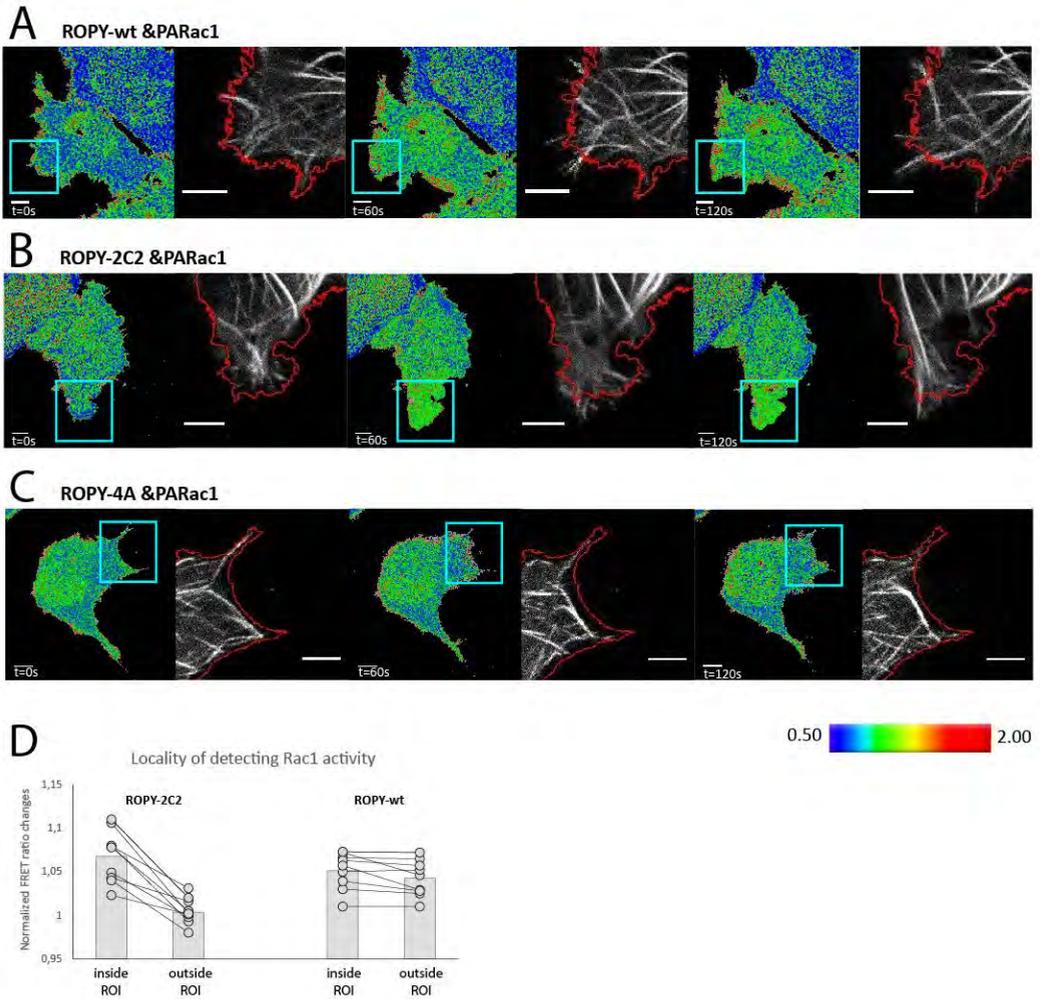
Fig 4. Locally affecting the tubulin affinity of ROPY. (A-C) Confocal images of ROPY variants with PARac1 & EB3-iRFP expressed in HEK293T cells. A) wt free diffusible ROPY with PARac1, B) membrane bound ROPY-2C2 with PARac1 and C) phosphorylation-deficient ROPY-4A with PARac1. The cells were locally illuminated with 458nm pulses every 20s within the ROI as indicated in blue. Subsequent microtubule changes are visualized in relation to the outline of the cell at t=0, indicated in red. The images are representative examples of n>10 observations. Scale bars represent 6 μm (D) HEK293T cells were co-transfected with PARac1 and either ROPY or ROPY-2C2, and locally illuminated with 458nm for 5 minutes. Normalized ratiometric FRET responses from within the activated ROI are plotted against the changes outside of that ROI, n=10.

Discussion

The applications for optogenetics are continuously increasing, however, not many supporting quantitative imaging tools are currently available for the technique. With FRET sensors for instance, the major issue is the spectral overlap of the excitation spectrum of most existing sensors with the activation spectrum of blue light responsive optogenetic domains, which renders both techniques incompatible with each other. Some have stated that single FP-based reporters might be the future of optogenetic readouts[33], however there are far less of these reporters currently available than FRET sensors, and most single FP-based sensors provide qualitative rather than quantitative readout. Thus at the moment the easiest way of obtaining a quantitative reporter that is compatible with blue responsive optogenetics is to alter the spectral properties of existing FRET probes. Recently, a few attempts have been made to solve this problem, e.g. adding bioluminescent protein donors to existing FRET sensors which rely on coelenterazine additives[34], or replacing the FPs with a new infrared FP pair[35]. However, these methods have certain practical disadvantages, as bioluminescence requires additives and is accompanied by low photon fluxes and the latter utilizes FPs in the far-red spectrum which to date still have sub-optimal properties for FRET[5,35], both hampering FRET sensing of subtle effects. Therefore, we decided to create a red-shifted FRET sensor with FPs in the 500nm+ excitation that exhibit high quantum yield and brightness in order to make the FRET pair compatible for sensors with lower dynamic ranges as well[7,8]. The original COPY sensor displayed a relatively low dynamic range, and our failed attempts at maintaining a functional sensor with orange and near-infrared FPs made it clear that an optimized FRET pair with the right spectral properties and a good acceptor FP is really required for low dynamic range sensors. Upon further screening, we identified the combination of sYFP2 as donor with mScI as acceptor to work well. We think that other yellow donors such as mVenus and mCitrine[36,37], not tested here will probably show similar results. Possibly, the higher quantum yield mNeongreen and mClover3[38,39] could be used as well, but we decided not to use these FPs as donors in view of their blue shift of ~10 nm as compared to sYFP2 which reduces the spectral overlap with the mScI acceptor and reduces the extinction coefficient at 514 nm with roughly 30-50%. In view of its efficient maturation, high brightness and long Förster radius for FRET from an sYFP2 donor (6.24 nm), mScI turned out to be the key element of the red-shifted ROPY sensor. The R125I mutation that reintroduces a dimerizing surface on the FP[25] was able to enhance the FRET contrast even further. Remarkably, we determined that this mutation did not stimulate intermolecular dimerization but that it increased only intramolecular FRET, probably by improving the binding affinity between the donor and acceptor FP of tubulin-free stathmin. The biological properties of the sensor were found to be unaltered by the red-shift. Its activity still depends on the change in tubulin affinity through phosphorylation, basal activity was highest at edge of the cells, and a decrease of tubulin incorporation into microtubules that scales with stathmin concentration was also observed, all just as reported for the original COPY sensor[9]. High concentrations of stathmin appeared to disrupt the basal FRET ratio (fig S2). As a result of

these concentration dependent effects we recommend to use the sensor only at low expression levels for accurate measurements and minimal modulation of the free tubulin concentration.

ROPY could be accurately measured independent of a PARac1 optogenetic construct, though the dynamic range was slightly lower and more variable as compared to paclitaxel stimulation. This is likely due to the basal activity of PARac1 in the dark state at varying concentrations, and the fact that phosphorylation is continuously being reversed in the cell by phosphatases while paclitaxel circumvents this pathway. Dark state activities are always present in optogenetic constructs[1,22], meaning this can always affect a FRET sensor's dynamic range paired with it. That is another reason why a FRET pair with optimized efficiency is preferred for optogenetic experiments. PARac1 induced the largest FRET change near the plasma membrane, which makes sense as Rac1 is known to be associated with the plasma membrane when it is activated[40]. Rac1 activation is most frequently discussed in the framework of the resulting lamellipodia and filopodia, which are attributed to downstream actin polymerization[29,41], though other components like the Rac1-PAK1 pathway can also clearly influence the resulting protrusions as we observed. When we looked at microtubule dynamics in response to a local induction of Rac1 activity, we detected microtubules extending into protrusions, which help to define their shape by acting as a rigid support structure. This response was only present in combination with the wildtype stathmin sensor, and not ROPY-4A, meaning the effect of stathmin and local tubulin availability is important when it comes to cell morphology and motility. It has previously been established that Rac1 activity is required to induce pioneer microtubules that occur at the leading cell edge[11], and our data suggests that the downstream regulatory mechanisms to achieve this could be as simple as regulating localized tubulin concentrations through stathmin for example. The fact that microtubules extending into protrusions occurred only within the targeted area means that tubulin dimers will quickly be incorporated in nearby microtubules when released, thus allowing a simple capture-and-release function to guide the cytoskeleton. The combination of PARac1 and ROPY-2C2 FRET sensing could be a great tool to further study the cytoskeletal effects of local free tubulin gradients by gaining spatio-temporal control over local tubulin concentrations with a sensory readout. The availability of the near-infrared part of the spectrum with this combination is highly valuable since it allows direct visualization of the elicited response.

By red-shifting the COPY sensor, we showed that it is possible convert existing FRET probes with low dynamic range into optogenetic-compatible ones. The sYFP2 and mScI-R125I fluorescent proteins are a great pair that allow for complete separation of control over blue light responsive protein domains and sensor readouts, while maintaining a solid dynamic FRET range. This approach adds to the possibilities of red-shifting sensors and will hopefully result in more studies combining FRET with optogenetically controlled signalling, since molecular information on spatio-temporally regulated systems could become an invaluable asset in future research.

Materials & Methods

<u>Plasmid constructs</u>

The original COPY sensor plasmid was a kind gift from Philippe Bastiaens. The protein coding part was first inserted into a pTriEx-3 plasmid backbone through AgeI and NotI restriction sites for easier cloning and expression purposes. Subsequent exchange of fluorescent proteins (FPs) was achieved by extracting the desired donor FPs from pClontech-FP-C1 plasmids with AgeI and BglII restriction sites. The acceptor FPs were amplified from pClontech-FP-C1 plasmids with forward primer 5'-TGATGGATCCGGTTCA(18xN) and reverse primer 5'-GATACCTGAGGGCGGCCGCTCATTT where 18xN represents the start of the specific protein sequences. The amplified domains were then inserted into the sensor plasmid through BamHI and Bsu36I restriction sites.

Generation of the phosphomimic (OP18-4E) and phosphoblock (OP18-4A) mutants of the stathmin sensor was achieved by introducing point mutations through the following primers: S16A/E: forward 5'-TGGAGAAGCGCGCT(GCA/GAA)GGCCAGGCTTTTG and reverse 5'-CAAAAGCCTGGCCTTCAGCGCGCTTCTCCA; S25A/E: forward 5'-GAGCTGATTCTC(GCC/GAA)CCTCGGTCAAAAG and reverse 5'-CTTTTGACCGAGGTTCGAGAATCAGCTC; S38A/E: forward 5'-CGATTTCCCCCTT(GCT/GAG)CCCCCAAAGAAG and reverse 5'-CTTCTTTGGGGGGCTCAAGGGGGAAATCG; S63A/E: forward 5'-GAAAGACGCAAG(GCT/GAA)CATGAGGCGGAAG and reverse 5'-CTTCCGCCTCATGTTCCTTGCGTCTTTC.

The R123I mutation in mScI was introduced through amplification with forward primer 5'-CAAGGTGAAGCTCATCGGCACCAACTTCCCTCC and reverse primer 5'-TAGATCAGGGTGCCGTCCTCCAGG. The Y67G mutation was introduced into sYFP2 through amplification with forward primer 5'-CCTCGTGACCACCCTGGGCGGCGGCGTGCAGTGCTTCG and reverse primer 5'-GTGGGCCAGGGCACGGGCAGCTTG, and the same mutation introduced into mScI with forward primer 5'-GTCCCCTCAGTTCATGGGCGGCTCCAGGGCCTTC and reverse primer 5'- AGGATGTCCCAGGAGAAGGGCAG.

The membrane-anchored version of ROPY was made by extracting the sensor domains with AgeI and SgrAI restriction sites for ligation into our previously published 2xC2 plasmid which is available through addgene (114416).

PA-Rac1 and α-tubulin-iRFP713 were obtained from addgene (22027 & 56277) (Cambridge, MA, USA).

We obtained EB3-GFP as a kind gift from Niels Galjart (Rotterdam, Erasmus MC), and EB3-iRFP was subsequently cloned by swapping the iRFP from α-tubulin-iRFP713 through AgeI and BsrGI restriction sites.

All relevant new generated constructs from this publication are available for use through addgene (ID 128002-128009).

Cell culture & transfection

Human embryonic kidney cells (Hek293, American Type Culture Collection crl-1573) and human HeLa cervical cancer cells (ccl-2) were cultured in Dulbecco's modified Eagle medium (DMEM) supplemented with Glutamax and 10% fetal bovine serum at 37°C and 7% CO_2. All cell culture media were obtained from Invitrogen (Breda, NL). For experiments, all cells were cultured on 25mm glass coverslips (Menzel- Gläser, Braunschweig, Germany) and transiently transfected with plasmids using 1 μg/ml polyethylenimine approximately 24h prior to imaging. Hek293 cells were serum starved for 4h before experiments. Right before imaging the culture medium was replaced with microscopy medium (137 mM NaCL, 5.4mM KCl, 1.8 mM $CaCl_2$, 0.8mM $MgCl_2$, 20mM glucose, and 20mM HEPES at PH = 7.4).

Widefield ratiometric FRET measurements

Hek293T cells were imaged on a widefield Zeiss Axiovert 200M microscope (Carl Zeiss MicroImaging, Jena, Germany) equipped with a 10x Plan Neofluar objective (NA 0.3 air) and a cooled charge-coupled device camera (Hamamatsu ORCA II). Cells were excited using a mecury lamp, at 500/20nm with a 535/30nm emission filter for YFP donor signal and a 620/60nm emission filter for RFP sensitized emission. For OFP donor signals, 500/20nm excitation was paired with a 572/28nm emission filter, while the near-infrared sensitized emission was excited with 500/20nm and detected by a 620/60nm emission filter. Regular acceptor intensities were obtained by 577/20 excitation with a 620/60nm emission filter. Cells were stimulated with a 1:1000 dilution of 10mM paclitaxel stock dissolved in DMSO (Sigma-Aldrich) and imaged again 1h after incubation. Background and flat-field corrections were applied to all images. Cells with RFP intensity counts above 200 were not analyzed in order to avoid artefacts in the FRET signal due to concentration. The RFP/YFP FRET ratio for each condition was obtained by calculating the slope of plotting $\Sigma(\text{donor} \times \text{SE}) / \Sigma(\text{donor}^2)$ for n>400. The error bars represent the 95% confidence intervals. Measurements were taken from distinct samples.

Confocal laser scanning microscopy

Experiments were performed on an inverted Leica TCS SP8 microscope (Leica Microsystems, Germany) equipped with a 63x HC Plan Apo objective (NA 1.4 oil) and HyD hybrid detectors at 37°C. YFP donor signals were obtained by exciting cells with a 514nm argon ion laser and detection with a 525-550nm emission bandpass. RFP sensitized emission signals were obtained by exciting cells with a 514nm argon ion laser and detection with a 590-625nm emission bandpass. iRFP signals were obtained by exciting cells with a 633nm helium-neon laser and detection with a 670-800nm emission bandpass.

Optogenetic activation was achieved by scanning an ROI of the desired size with a 458nm argon ion laser line at 40 µW per pixel, repeated every 20s.

Images were analyzed using ImageJ (National Institutes of Health, Bethesda, MD) for background corrections, calculating RFP/YFP ratio images (fig 2C, 3A, 4A), creating overlays of cell outlines (fig 4A), and separating a 5 µm thick outer circumference of cells from the remaining core (fig 3B). Measurements were taken from distinct samples.

Abbreviations

AsLOV2	Avena sativa Light-Oxygen-Voltage-sensing domain 2
COPY	CFP-OP18/Stathmin-YFP (FRET sensor)
DMSO	Dimethyl sulfoxide
EB3	End-binding protein 3
FP	Fluorescent protein
FRET	Förster Resonance Energy Transfer
HEPES	N-2-hydroxyethylpiperazine-N-ethanesulfonic acid
OP18	Oncoprotein 18
PA-Rac1	Photo-activatable Rac1
ROPY	RFP-OP18/Stathmin-YFP (FRET sensor)
ROPY-4A	ROPY - S16A; S25A; S38A; S63A
ROPY-4E	ROPY - S16E; S25E; S38E; S63E

Acknowledgements

Author contributions

O.G., S.C. and T.G. conceived and planned the experiments. O.G. and S.C. performed the experimental work. O.G. and T.G. wrote the manuscript in consultation with S.C.

Data availability

The underlying datasets from figures in this publication are available from the corresponding author on reasonable request.

Competing interests

This research was conducted without any competing interests.

References

1. Zhang, K., & Cui, B. (2015). Optogenetic control of intracellular signaling pathways. *Trends in biotechnology*, *33*(2), 92-100.

2. Rost, B. R., Schneider-Warme, F., Schmitz, D., & Hegemann, P. (2017). Optogenetic tools for subcellular applications in neuroscience. *Neuron*, *96*(3), 572-603.

3. Deiters, A. (2018). Special Issue on Optochemical and Optogenetic Control of Cellular Processes. *ChemBioChem*, *19*(12), 1198-1200.

4. Kim, B., & Lin, M. Z. (2013). Optobiology: optical control of biological processes via protein engineering.

5. Day, R. N., & Davidson, M. W. (2012). Fluorescent proteins for FRET microscopy: monitoring protein interactions in living cells. *Bioessays*, *34*(5), 341-350.

6. van der Krogt, G. N., Ogink, J., Ponsioen, B., & Jalink, K. (2008). A comparison of donor-acceptor pairs for genetically encoded FRET sensors: application to the Epac cAMP sensor as an example. *PloS one*, *3*(4), e1916.

7. Bindels, D. S., Haarbosch, L., Van Weeren, L., Postma, M., Wiese, K. E., Mastop, M., ... & Gadella Jr, T. W. (2017). mScarlet: a bright monomeric red fluorescent protein for cellular imaging. *Nature methods*, *14*(1), 53.

8. Bajar, B., Wang, E., Zhang, S., Lin, M., & Chu, J. (2016). A guide to fluorescent protein FRET pairs. *Sensors*, *16*(9), 1488.

9. Niethammer, P., Bastiaens, P., & Karsenti, E. (2004). Stathmin-tubulin interaction gradients in motile and mitotic cells. *Science*, *303*(5665), 1862-1866.

10. Belmont, L. D., & Mitchison, T. J. (1996). Identification of a protein that interacts with tubulin dimers and increases the catastrophe rate of microtubules. *Cell*, *84*(4), 623-631.

11. Wittmann, T., Bokoch, G. M., & Waterman-Storer, C. M. (2003). Regulation of leading edge microtubule and actin dynamics downstream of Rac1. *The Journal of cell biology*, *161*(5), 845-851.

12. Curmi, P. A., Andersen, S. S., Lachkar, S., Gavet, O., Karsenti, E., Knossow, M., & Sobel, A. (1997). The stathmin/tubulin interaction in vitro. *Journal of Biological Chemistry*, *272*(40), 25029-25036.

13. Howell, B., Larsson, N., Gullberg, M., & Cassimeris, L. (1999). Dissociation of the tubulin-sequestering and microtubule catastrophe-promoting activities of oncoprotein 18/stathmin. *Molecular biology of the cell*, *10*(1), 105-118.

14. Cassimeris, L. (2002). The oncoprotein 18/stathmin family of microtubule destabilizers. *Current opinion in cell biology*, *14*(1), 18-24.

15. Sobel, A. (1991). Stathmin: a relay phosphoprotein for multiple signal transduction?. *Trends in biochemical sciences*, *16*, 301-305.

16. Di Paolo, G., Antonsson, B., Kassel, D., Riederer, B. M., & Grenningloh, G. (1997). Phosphorylation regulates the microtubule-destabilizing activity of stathmin and its interaction with tubulin. *FEBS letters*, *416*(2), 149-152.

17. Daub, H., Gevaert, K., Vandekerckhove, J., Sobel, A., & Hall, A. (2001). Rac/Cdc42 and p65PAK regulate the microtubule-destabilizing protein stathmin through phosphorylation at serine 16. *Journal of Biological Chemistry*, *276*(3), 1677-1680.

18. Steinmetz, M. O. (2007). Structure and thermodynamics of the tubulin–stathmin interaction. *Journal of structural biology*, *158*(2), 137-147.

19. Andersen, S. S., Ashford, A. J., Tournebize, R., Gavet, O., Sobel, A., Hyman, A. A., & Karsenti, E. (1997). Mitotic chromatin regulates phosphorylation of Stathmin/Op18. *Nature*, *389*(6651), 640.

20. Desai, A., & Mitchison, T. J. (1997). Microtubule polymerization dynamics. *Annual review of cell and developmental biology*, *13*(1), 83-117.

21. Larsson, N., Segerman, B., Gradin, H. M., Wandzioch, E., Cassimeris, L., & Gullberg, M. (1999). Mutations of oncoprotein 18/stathmin identify tubulin-directed regulatory activities distinct from tubulin association. *Molecular and cellular biology*, *19*(3), 2242-2250.

22. Wu, Y. I., Frey, D., Lungu, O. I., Jaehrig, A., Schlichting, I., Kuhlman, B., & Hahn, K. M. (2009). A genetically encoded photoactivatable Rac controls the motility of living cells. *Nature*, *461*(7260), 104.

23. Nguyen, A. W., & Daugherty, P. S. (2005). Evolutionary optimization of fluorescent proteins for intracellular FRET. *Nature biotechnology*, *23*(3), 355.

24. Kremers, G. J., Goedhart, J., van Munster, E. B., & Gadella, T. W. (2006). Cyan and yellow super fluorescent proteins with improved brightness, protein folding, and FRET Förster radius. *Biochemistry*, *45*(21), 6570-6580.

25. Campbell, R. E., Tour, O., Palmer, A. E., Steinbach, P. A., Baird, G. S., Zacharias, D. A., & Tsien, R. Y. (2002). A monomeric red fluorescent protein. *Proceedings of the National Academy of Sciences*, *99*(12), 7877-7882.

26. Beretta, L., Dobransky, T., & Sobel, A. (1993). Multiple phosphorylation of stathmin. Identification of four sites phosphorylated in intact cells and in vitro by cyclic AMP-dependent protein kinase and p34cdc2. *Journal of Biological Chemistry*, *268*(27), 20076-20084.

27. Raftopoulou, M., & Hall, A. (2004). Cell migration: Rho GTPases lead the way. *Developmental biology*, *265*(1), 23-32.

28. Filonov, G. S., Piatkevich, K. D., Ting, L. M., Zhang, J., Kim, K., & Verkhusha, V. V. (2011). Bright and stable near-infrared fluorescent protein for in vivo imaging. Nature biotechnology, 29(8), 757.

29. de Curtis, I., & Meldolesi, J. (2012). Cell surface dynamics–how Rho GTPases orchestrate the interplay between the plasma membrane and the cortical cytoskeleton. J Cell Sci, 125(19), 4435-4444.

30. Van Geel, O., Hartsuiker, R., & Gadella, T. W. (2018). Increasing spatial resolution of photoregulated GTPases through immobilized peripheral membrane proteins. *Small GTPases*, 1-10.

31. Yeung, T., Gilbert, G. E., Shi, J., Silvius, J., Kapus, A., & Grinstein, S. (2008). Membrane phosphatidylserine regulates surface charge and protein localization. *Science*, *319*(5860), 210-213.

32. Stepanova, T., Slemmer, J., Hoogenraad, C. C., Lansbergen, G., Dortland, B., De Zeeuw, C. I., ... & Galjart, N. (2003). Visualization of microtubule growth in cultured neurons via the use of EB3-GFP (end-binding protein 3-green fluorescent protein). *Journal of Neuroscience*, *23*(7), 2655-2664.

33. Kim, J., & Do Heo, W. (2018). Synergistic Ensemble of Optogenetic Actuators and Dynamic Indicators in Cell Biology. Molecules and cells, 41(9), 809.

34. Komatsu, N., Terai, K., Imanishi, A., Kamioka, Y., Sumiyama, K., Jin, T., ... & Matsuda, M. (2018). A platform of BRET-FRET hybrid biosensors for optogenetics, chemical screening, and in vivo imaging. *Scientific reports*, *8*(1), 8984.

35. Shcherbakova, D. M., Cammer, N. C., Huisman, T. M., Verkhusha, V. V., & Hodgson, L. (2018). Direct multiplex imaging and optogenetics of Rho GTPases enabled by near-infrared FRET. *Nature chemical* biology, 14(6), 591.

36. Nagai, T., Ibata, K., Park, E. S., Kubota, M., Mikoshiba, K., & Miyawaki, A. (2002). A variant of yellow fluorescent protein with fast and efficient maturation for cell-biological applications. Nature biotechnology, 20(1), 87.

37. Shaner, N. C., Steinbach, P. A., & Tsien, R. Y. (2005). A guide to choosing fluorescent proteins. Nature methods, 2(12), 905.

38. Shaner, N. C., Lambert, G. G., Chammas, A., Ni, Y., Cranfill, P. J., Baird, M. A., ... & Davidson, M. W. (2013). A bright monomeric green fluorescent protein derived from Branchiostoma lanceolatum. Nature methods, 10(5), 407.

39. Bajar, B. T., Wang, E. S., Lam, A. J., Kim, B. B., Jacobs, C. L., Howe, E. S., ... & Chu, J. (2016). Improving brightness and photostability of green and red fluorescent proteins for live cell imaging and FRET reporting. Scientific reports, 6, 20889.

40. del Pozo, M. A., Alderson, N. B., Kiosses, W. B., Chiang, H. H., Anderson, R. G., & Schwartz, M. A. (2004). Integrins regulate Rac targeting by internalization of membrane domains. Science, 303(5659), 839-842.

41. Bisi, S., Disanza, A., Malinverno, C., Frittoli, E., Palamidessi, A., & Scita, G. (2013). Membrane and actin dynamics interplay at lamellipodia leading edge. Current opinion in cell biology, 25(5), 565-573.
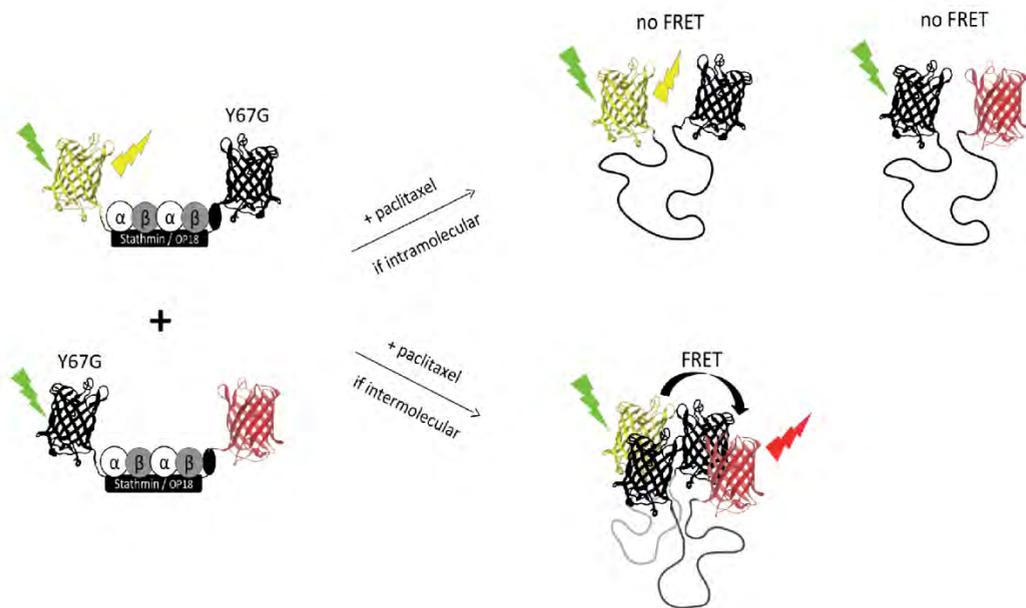
Supplemental Materials

Fig S1. Assessment of altered FP binding affinities due to the R125I point mutation. Schematic overview of the experiment performed in fig 2A, depicting both possible outcomes. We introduced a Y67G point mutation into either FP in order to create inactive versions of ROPY with one non-fluorescent FP-protein structure and one functional sYFP2 or mScI. By themselves these ROPY mutants cannot undergo a FRET interaction upon release of tubulin. However, if the dimerizing R125I mutation introduced into mScI would have a much higher affinity for itself than for differently constructed FP ß-barrels, it could stimulate intermolecular binding which would allow for an intermolecular FRET interaction to occur. Since no FRET was detected during the experiment in fig 2A, we have to assume that the R125I mutation increased ROPY's dynamic range mostly by promoting intramolecular FP interactions.
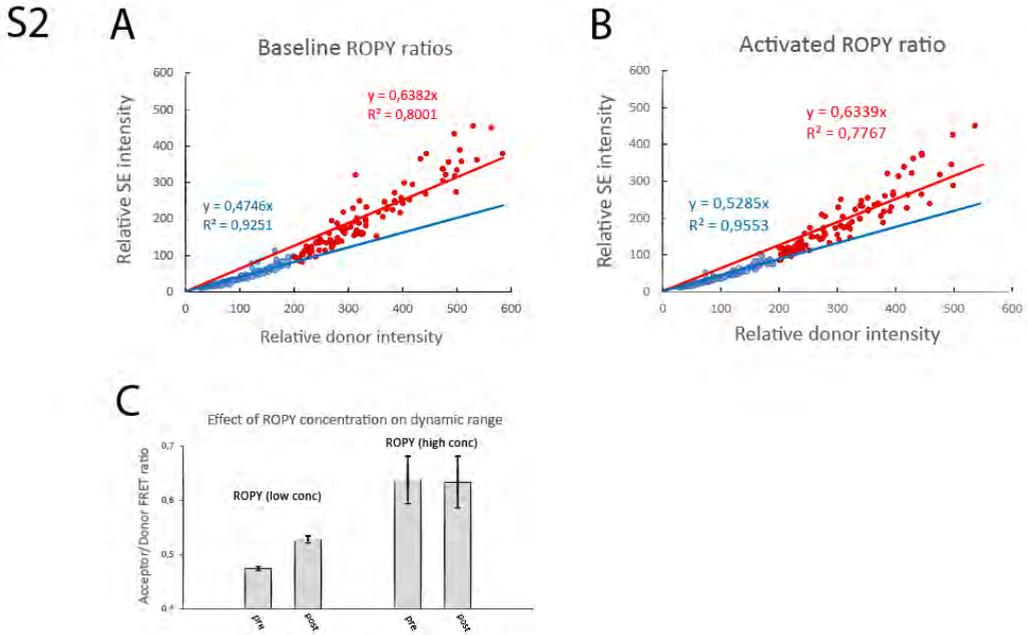
Fig S2. Concentration dependence of ROPY's FRET ratio. (A-B) Individual donor and sensitized emission intensities of basal ROPY (A) and paclitaxel stimulated ROPY (B) are plotted to indicate the effect of sensor concentration on the FRET dynamic range. We arbitrarily set a threshold at a relative donor intensity of 200 since on average the points start to deviate from a linear correlation above this threshold. Cells used in the main analysis are represented in blue and excluded ones in red. The average ratio for each fraction was determined by the slope of their respective trendlines, which has a large error for red points due to the wide spread of FRET ratios at these concentrations. This variation likely reflects the variability in free tubulin concentrations between those cells, which can alter the 2:1 binding ratio with stathmin and disrupt the basal non-FRET state. (C) RFP/YFP ratiometric FRET comparison of high and low ROPY expression levels, both before and after addition of 10 μM paclitaxel. Values were obtained from the trendlines in A-B. The ROPY sensor was transiently expressed in HEK293T. Error bars indicate the 95% confidence intervals.
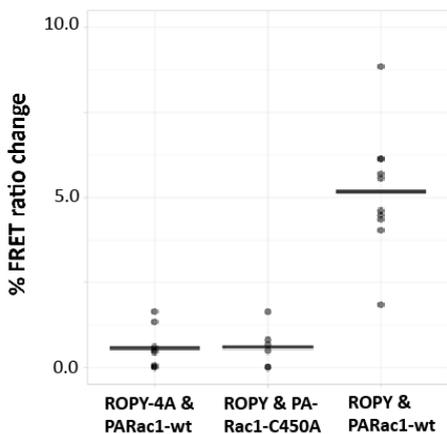
S3

Fig S3. Effect of PA-Rac1 on stathmin. Relative FRET ratio increase of ROPY & PARac1-wt, compared to ROPY & inactive PARac1-C450A, as well as inactive ROPY-4A & PARac1-wt. Without either a phosphorylatable stathmin domain or an active Rac1, no significant FRET change was observed. This confirms that PA-Rac1 is able to indirectly regulate the tubulin binding activity of stathmin. Experiment was performed in HeLa cells under 5 minutes exposure to 458nm light, n=8.
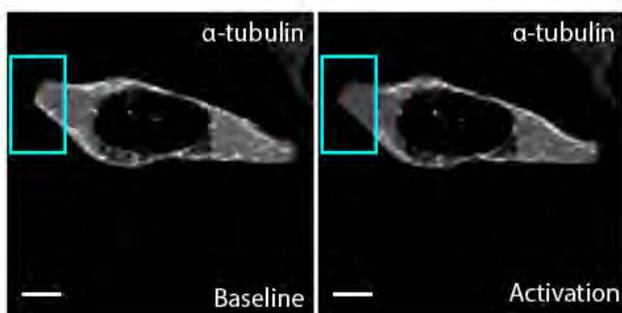
S4

Fig S4. Visualization of ROPY-2C2's tubulin binding ability. In fig 4B we showed that confining ROPY to the plasma membrane resulted in a more local FRET response which correlated nicely with the area where we induced local PA-Rac1 activation. Here we wanted to visually confirm that this more precise spatial representation of Rac1 activity was due to local phosphorylation of stathmin, which is why we co-expressed PA-Rac1, ROPY-2C2, and α-tubulin-iRFP713. We found that local PA-Rac1 activation with 458nm within the blue ROI, trigged the release of bound tubulin within that ROI but not elsewhere, which confirms that ROPY-2C2 can be used as an indicator of locally released tubulin dimers. Experiment was performed with HEK293T cells.
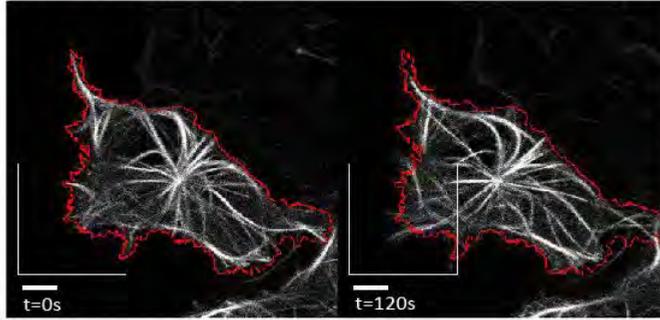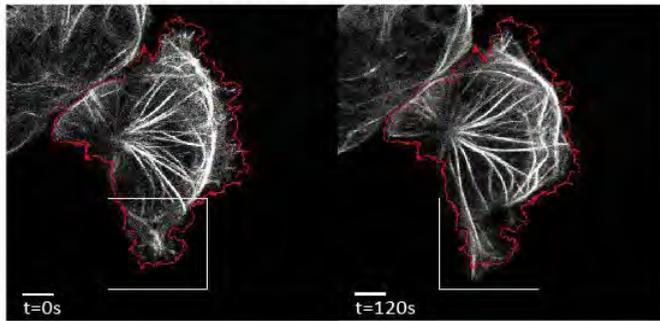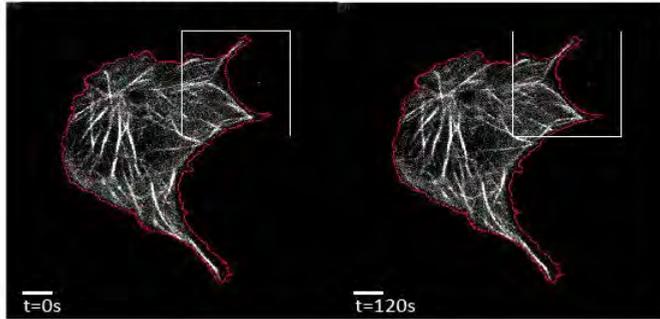
Fig S5. Visualization of ROPY-2C2's tubulin binding ability. (A-C) Whole cell confocal images of EB3-iRFP expressed in HEK293T cells together with A) wt free diffusible ROPY & PA-Rac1 B) membrane bound ROPY-2C2 & PA-Rac1 and C) phosphorylation-deficient ROPY-4A & PA-Rac1. These images are the same as in fig 4A-C except that here the microtubule composition of the entire cells are visible. These enlarged images clearly show that microtubule extensions into the lamellipodia only occurred within the area of PA-Rac1 activation and subsequent tubulin release. The fact that any protrusions outside the ROI don't show microtubule extensions suggests that the released tubuluin will quickly become incorporated into nearby growing microtubules. The cells were locally illuminated with 458nm pulses every 20s within the ROI as indicated. For reference, the outline of the cell at t=0 is indicated in red. The images are representative examples of n>10 observations. Scale bars represent 6 μm.